SRC-TR 87-109

Multiple Operator Deconvolution with Additive Noise; The Envelope Operator

by

Carlos A. Berenstein
E. Vincent Patrick

MULTIPLE OPERATOR DECONVOLUTION WITH ADDITIVE NOISE: THE ENVELOPE OPERATOR

CARLOS A. BERENSTEIN

E. VINCENT PATRICK

MAY 8, 1987

This research was supported by the Systems Research Center, University of Maryland, under grant NSF-CDR-8500108

Abstract

The methods for multiple operator deconvolution of Berenstein, Taylor, and Yger are examined for the case of the addition of a noise signal after each of the multiple convolutions and preceding the deconvolutions. It is shown that for strongly coprime multiple operators there is an obvious choice for optimal deconvolvers. The case of m strongly coprime, parallel convolvers with m independent noise sources is compared to m identical, parallel convolvers with m independent, identically distributed noise sources. A performance criterion is defined. The performance for selected collections of strongly coprime convolvers is shown to be at least as good as that for the corresponding collection of an equal number of identical, parallel convolvers. That is, there is no penalty for the additional frequency response available with deconvolution, at least for the noncompactly supported optimal deconvolvers. Qualitative methods are developed to characterize the properties of strongly coprime configurations. These methods enable the description of circumstances in which it is advantageous to use strongly coprime multiple detectors of large support.

INTRODUCTION

Throughout the last several years mathematical results have been presented [1-8] which form the foundations for the use of multiple (parallel) linear operators, each given by convolution with a distinct kernel (or impulse response), in place of the use of a single such linear operator or, equivalently, in place of the use of multiple (parallel) operators each with the identical kernel. (See Figure 1.) In the multiple operator method each distinct kernel (alternately called a convolver or convolutor) is associated with a second kernel, referred to as a deconvolver. The utility of this is that if the convolvers have compact support and satisfy certain conditions then there exists associated deconvolvers that also have compact support and for which the overall linear operator defined by the sum of the convolutions of each convolver-deconvolver pair is equivalent to the identity operator. This is more concisely stated when the kernels are considered as distributions, that is, as linear functionals on the space of infinitely differentiable functions on $\mathbb{R}^n$. The mathematical results cited above describe the conditions under which compactly supported distributions $\mu_1, \mu_2, \ldots, \mu_m$ have associated to them compactly supported distributions $\nu_1, \nu_2, \ldots, \nu_m$ such that

$$\sum_{i=1}^{m} \mu_i * \nu_i = \delta \ , \tag{1}$$

where δ is the Dirac distribution on $\mathbb{R}^n$ and where * denotes convolution.

This is of interest for applications in which the convolver μ_i must correspond to a physical, analog device wherein the impulse response is dictated by a solid state or biological process. It is entirely possible to select such analog convolvers which satisfy approximately the multiple operator criteria. Then each associated deconvolver can be digitally

implemented. The fact that the deconvolvers are linear and of compact support means that their implementation is straightforward; that they are continuous implies stability. Most importantly, the evident high bandwidth of the overall operator is accomplished without any essential change in the response functions of the analog devices. The term overall operator refers to the operator given by the kernel distribution $\sum_{i=1}^{m} \mu_i * \nu_i = \delta$. Of course, because of practical constraints, such as analog and digital approximations and computation time, the design objective for the overall operator would not be the identity operator with impulse response δ but rather a high bandwidth approximation of the identity operator given by an impulse response ϕ. In terms of the distribution equation (1) and since convolutions commute

$$\sum_{i=1}^{m} (\mu_i * \phi) * \nu_i = \sum_{i=1}^{m} \mu_i * (\nu_i * \phi) = \phi \ . \tag{2}$$

In a sense ϕ can be considered to be made up of "parts," each of which arises from one of the practical constraints just listed, along with a special part that is deliberately added to control the noise power spectrum of the output of the overall operator.

The publications on this subject have appeared primarily in the mathematical literature. The following issues regarding (1) have been addressed: sufficient conditions for the existence of solutions [1-4]; examples of sets of distributions that satisfy the sufficient conditions [5,6]; construction of explicit solutions, that is, explicit formulas for the deconvolvers [7,8]; and construction and evaluation of approximate solutions [9,10].

Only recently have specific applications of (1) been mentioned. The case of one dimensional integration over an interval as a linear operator on a variety of function spaces has been presented.[9] This was the first time

that (1) and contemporary mathematical methods for understanding the equation were applied to physical problems. There the linear operators in (1) were considered to act on function spaces other than $C^{\infty}(\mathbb{R}^n)$. The consideration of (1) acting on $L^p(\mathbb{R}^n)$ or $H^p(\mathbb{R}^n)$ requires the consideration of $C^{\infty}(\mathbb{R}^n)$ as a dense subset and the behavior of the operators on the closure. Consequently it is natural that approximate identities and mollifiers such as ϕ in (2) are used. Also discussed in [9] were the question of additive noise and the question of the continuity of the overall operator with respect to the distributions $\mu_1, \mu_2, \ldots, \mu_m$. The noise question is in regard to noise added following the action of the operators defined by the μ_i, while the continuity question is in regard to the dependence of the overall performance on either the actual analog approximations of the μ_i or the digital approximations of the ν_i.

Following the appearance of [9], two-dimensional computer simulations were performed to demonstrate (2) for imaging devices wherein the analog convolvers were solid state photodetectors. In conjunction with the simulation, approximation methods for some specific solutions [10] were analyzed. In the following year, as specific application were considered, more of the methods of systems analysis were merged into the developments and, besides detectors, a sequence of operators was considered, wherein each operator was a multiple operator type.

This paper describes the result of our application of standard methods of linear systems and random signals to the multiple operator type of system of equations (1) and (2). This analysis was necessary if one was to seriously consider multiple operator designs. While the extended bandwidth was well understood, analyzed, and even demonstrated in simulations, the consequence of the introduction of noise and of design errors was not fully understood. It

was clear that since the operator was linear and continuous that there would be no instablity due to noise (at least for smooth ($C^{\infty}(\mathbb{R}^n)$) approximations), which is already an improvement over the case of single operator reconstruction methods [6,9]. However, the performance needed to be explicity described so that standard tools such as resolution, equivalent bandwidth, and signal to noise ratio would be available for systems engineering design studies.

This investigation was motivated in large part by the potential application of these multiple operator methods to electo-optics, especially to imaging devices. We have in mind imaging devices that are for the detection, transformation, and display of electromagnetic radiation for a human observer as well as such devices for artificially intelligent "observers." Consequently, the problems and the desired solutions have the flavor of this application. While the analysis and the results are in a sense general, much is framed and guided by the motivating problems.

With this in mind, let us reexamine our objective, stated just above, of performance descriptions suitable for use in engineering studies. For imaging electro-optics systems it is best to cast off any hope and preference, common in mathematics, for an obvious choice of norm or metric as a performance measure. First, performance criteria are never uniquely determined by the device: they depend instead on the infinite number of possible end-uses. Loosely speaking, if there are two end-uses that are "linearly independent," then one would need at least either two real valued performance metrics or a performance criterion that takes values in a 2-dimensional space. For example [11], for field use of an infrared imaging device for observations in a natural terrain, there is a requirement for good sensitivity at low spatial

frequencies for purposes of orientation and search strategy relative to the terrain, while there is a requirement for sufficient response at sufficiently high spatial frequencies for purposes of accomplishing the objective of the observation. These two sub-uses of field use are an example of two "independent" uses. A different end-use, say industrial robot vision, would surely have distinct sub-uses that were independent of those in the field use example.

The simplest thing to hope for is a performance criteria that can be "projected" onto any of the criteria "spanned" by a set of end-uses. Consequently, it is typical in electo-optics to use functions to characterize devices and systems and to rarely be satisfied with a choice of norm of the function, or even with a choice of a projection of the function to a finite dimensional space. In other words, one is willing to forego a linear ordering of devices. Even when a specific end-use is selected, a norm is still largely unsatisfactory.

GENERAL RESULTS

A fundamental result in this subject is the following. Given a set of distributions $\mu_1, \mu_2,\ldots,\mu_m$ on $\mathbb{R}^n$, each with compact support, then the necessary and sufficient condition for the existence of a second set of distributions $\nu_1, \nu_2,\ldots,\nu_m$ on $\mathbb{R}^n$, again each with compact support, such that

$$\sum_{i=1}^{m} \mu_i * \nu_i = \delta \ , \tag{1}$$

is that the Fourier-Laplace transforms of the μ_i, denoted $\hat{\mu}_i$, satisfy

$$\sum_{i=1}^{m} |\hat{\mu}_i(z)| \geq C_1 e^{-C_2 |\mathrm{Im}\ z|} (1+|z|)^{-N} \ , \quad z \in \mathbb{C}^n \tag{3}$$

for some positive constants C_1, C_2, and N.[5-7] (For $\zeta = (\zeta_1, \zeta_2,\ldots,\zeta_n) \in \mathbb{C}^n$ define $|\zeta| = \left(\sum_i |\zeta_i|^2 \right)^{1/2}$.) The condition (3) is often referred to as the *strongly coprime* condition.

Here we will need only elementary harmonic analysis and we shall consider the Fourier transform on $\mathbb{R}^n$, that is, the restriction of the Fourier-Laplace transform to $\mathbb{R}^n \subset \mathbb{C}^n$ in the sense that for $z = (z_1, z_2,\ldots,z_n) \in \mathbb{C}^n$, $\omega = (\omega_1, \omega_2,\ldots, \omega_n) = (\mathrm{Re}\ z_1, \mathrm{Re}\ z_2,\ldots, \mathrm{Re}\ z_n) \in \mathbb{R}^n$. Then (3) has the form

$$\sum_{i=1}^{m} |\hat{\mu}_i(\omega)| \geq C_1 (1+|\omega|)^{-N} \ , \quad \omega \in \mathbb{R}^n \tag{4}$$

For any distribution ν of compact support, $\hat{\nu} \in C^\infty(\mathbb{R}^n)$. As usual, we may choose $\phi \in C^\infty(\mathbb{R}^n)$ such that $\hat{\phi}$ has compact support and is sufficiently differentiable so that $\nu * \phi \in L^1(\mathbb{R}^n)$. But $\nu * \phi$ can not have compact support. However, for each i=1,2,...m define $h_i = \nu_i * \phi \in L^1(\mathbb{R}^n)$. Then

$$\sum_i \mu_i * h_i = \phi . \tag{5}$$

The $h_i \in L^1(\mathbb{R}^n)$ that satisfy (5) are not uniquely determined. In fact, from (4) and from $\hat{\mu}_i \in C^\infty(\mathbb{R}^n)$ and with ϕ as above,

$$D_i(\omega) = \frac{\bar{\hat{\mu}}_i(\omega)}{\sum_{j=1}^{m} |\hat{\mu}_j(\omega)|^2} \quad , \quad \hat{h}_i(\omega) = D_i(\omega)\hat{\phi}(\omega) \quad , \quad i=1,2,\ldots,m, \tag{6}$$

defines functions $h_i \in L^1(\mathbb{R}^n)$ which satisfy (5). ($\bar{z}$ denotes the complex conjugate of z.)

While (6) is exhibited essentially by inspection, the result can be obtained in a more systematic fashion as well as in a more general form. We first recall some standard tools, apply these tools to a simple case, and then proceed to the more general form. The diagram in Figure 2 represents an operator L acting on a function f. Let (temporarily) $f \in C^{\infty}(\mathbb{R}^n)$. Let $\mu_1, \mu_2, \ldots, \mu_m$ be an arbitrary set of m distributions with compact support. To each linear operator defined by μ_i let η_i be a sample function of a zero mean, wide-sense stationary randon process that is added to the output, and let N_i^2 ($N_i \geq 0$) be the noise power spectral density of the process. For each distinct i and j let η_i be independent of η_j and let each η_j be independent of f. The ν_i are defined in the sense that $(\nu_i * \phi)^{\wedge} = D_i\hat{\phi}$, where $\hat{\phi}$, $D_i \in C^r(\mathbb{R}^n)$, $\hat{\phi}$ has compact support, and r is sufficient for $\left(D_i\hat{\phi}\right)^{\wedge} \in L^1(\mathbb{R}^n)$. With this $g \in L^{\infty}(\mathbb{R}^n)$ is defined by ($\eta_i \in L^{\infty}(\mathbb{R}^n)$)

$$g = Lf = \sum_{i=1}^{m} (\mu_i * f + \eta_i) * (\nu_i * \phi). \tag{7}$$

In the usual manner, with E denoting expectation,

$$E\{g\} = \sum_{i=1}^{m} \mu_i * f * (\nu_i * \phi) \tag{8}$$

and for $T'_y(x) = x + y$, $^{\vee}$ denoting inverse Fourier transform, $\| \ \|_p$ the L^p norm

$$E\left\{\left(g - E\{g\}\right)\left(g - E\{g\}\right) \circ T'_y\right\} = \left[\sum_{i=1}^{m} N_i^2 |D_i|^2 |\hat{\phi}|^2\right]^{\vee}(y) \ , \tag{9a}$$

$$E\left\{\left(g - E\{g\}\right)^2\right\} = \frac{1}{(2\pi)^n}\left\|\sum_{i=1}^{m} N_i^2 |D_i|^2 |\hat{\phi}|^2\right\|_1 . \tag{9b}$$

The simplest configuration for L is all distributions equal, all deconvolvers trivial, and all random processes identically distributed:

$$\mu_i = \mu_0 \ , \quad \nu_i = \delta \ , \quad N_i^2 = N_0^2 \ , \quad \text{for } i = 1,2,\ldots,m \ . \tag{10}$$

Then

$$E\{g\} = m\mu_0 * \phi * f \ , \quad E\left\{\left(g - E\{g\}\right)^2\right\} = \frac{m}{(2\pi)^n}\left\| N_0 \, |\hat{\phi}| \right\|_2^2 \ . \tag{11}$$

The utility of (8) and (9) or of (11) is that if L is followed by a linear operator U with kernel u (which could model a specific end-use) then classical discrimination methods would compare (using (11) for illustration) the function

$$\left(U(E\{g\})\right)^2 = E\{Ug\}^2 = \left(u*(m\mu_0*\phi*f)\right)^2 = m^2\left[\left(\hat{u}\hat{\mu}_0\hat{\phi}\hat{f}\right)^{\vee}\right]^2 \tag{12}$$

$$\leq \left(\frac{m}{(2\pi)^n}\left\|\hat{u}\hat{\mu}_0\hat{\phi}\hat{f}\right\|_1\right)^2$$

$$\leq \left(\frac{m}{(2\pi)^n}\right)^2 \left\|\hat{u}\hat{\mu}_0\hat{\phi}\right\|_2^2 \left\|\hat{f}\right\|_2^2 \quad \text{when } f \in L^2(\mathbb{R}^n)$$

with the constant function

$$E\left\{\left(U\left(g - E\{g\}\right)\right)^2\right\} = \frac{m}{(2\pi)^n}\left\|\hat{u}N_0\hat{\phi}\right\|_2^2 \ . \tag{13}$$

The function $E\{Ug\}$ is referred to as the signal, $E\{Ug\}^2$ is referred to as the signal power or energy, and $E\left\{\left(U\left(g - E\{g\}\right)\right)^2\right\}$ is referred to as the noise power. Typically the ratio of $E\{Ug\}^2$ to $E\left\{\left(U\left(g - E\{g\}\right)\right)^2\right\}$ is considered, or, alternately, the positive square root of the ratio. Here we shall consistently use the later. If this ratio is evaluated at some distinguished point, the value defines a "signal to noise ratio." We denote by $\mathfrak{P}$ the projection of a function by the evaluation of the absolute value of the

function at the distinguished point. Given L and for a given choice of ϕ, f, $\mathcal{U}$, and $\mathcal{P}$ define

$$\mathcal{PNR}(\mathcal{U}L) = \frac{\mathcal{P}\mathcal{U}(E\{g\})}{\left[E\left\{\left(\mathcal{U}(g-E\{g\})\right)^2\right\}\right]^{1/2}} . \tag{14}$$

For a fixed choice of ϕ, f, $\mathcal{U}$, and $\mathcal{P}$ two operators L and L′ can be compared and ordered by (14).

On the other hand, for a choice of ϕ, f, $\mathcal{U}$, and $\mathcal{P}$, (14) is determined for the case of the trivial operator in (10) by the pair of functions

$$m\,\hat{\mu}_0 \text{ and } \sqrt{m}\,N_0 . \tag{15}$$

In general, let operators L and L′ have transfer functions and noise power spectral densities $\hat{\mu}$, N^2 and $\hat{\mu}'$, N'^2, respectively. For a choice of $\mathcal{U}$ we shall say that $\mathcal{U}L \,|\, \mathcal{U}L'$ (i.e.,"$\mathcal{U}L$ divides $\mathcal{U}L'$") if there exists a function $\hat{m} \in L^\infty(\mathbb{R}^n)$ such that $\hat{u}\,\hat{m}\,\hat{\mu} = \hat{u}\,\hat{\mu}'$. If $\mathcal{U}L \,|\, \mathcal{U}L'$ and $|\hat{m}|^2 |\hat{u}|^2 N^2 \le |\hat{u}|^2 N'^2$, we say that $\mathcal{U}L \ge \mathcal{U}L'$.

This definition is motivated by the following. As usual, let ϕ be such that a linear operator $\mathcal{M}$ with kernel m can be associated with $\hat{m}$ by considering $\hat{m}\hat{\phi}$. Let $\mathcal{B}$ be any continuous linear operator. For fixed $\mathcal{U}$ if $\mathcal{U}L \ge \mathcal{U}L'$ then $\frac{\mathcal{PNR}(\mathcal{U}\mathcal{B}\mathcal{M}L)}{\mathcal{PNR}(\mathcal{U}\mathcal{B}L')} \ge 1$. Consequently, $\sup_{\mathcal{B}} \mathcal{PNR}(\mathcal{U}\mathcal{B}L) \ge \sup_{\mathcal{B}} \mathcal{PNR}(\mathcal{U}\mathcal{B}L')$.

Next consider the operator L diagrammed in Figure 2 for the case in which $\mu_1, \mu_2, \ldots, \mu_m$ are distinct and strongly coprime (i.e., satisfy (3)). An obvious consequence is $\sum_{i=1}^{m} |\hat{\mu}_i(\omega)|^2 > 0$ and, equivalently,

$$0 \neq (\hat{\mu}_1(\omega), \hat{\mu}_2(\omega), \ldots, \hat{\mu}_m(\omega)) \in \mathbb{C}^n , \quad \omega \in \mathbb{R}^n . \tag{16}$$

Consequently we can visualize (16) as is shown in Figure 3*a*. A similar illustration can be used to visualize $\hat{f}(\omega)(\hat{\mu}_1(\omega), \hat{\mu}_2(\omega), \ldots, \hat{\mu}_m(\omega)) = (\hat{f}(\omega)\hat{\mu}_1(\omega), \hat{f}(\omega)\hat{\mu}_2(\omega), \ldots, \hat{f}(\omega)\hat{\mu}_m(\omega))$, except the "curve" passes through the

origin if and only if $\hat{f}(\omega) = 0$. The power spectral densities are real and nonnegative (thus we write N_i^2 and choose $N_i \geq 0$). Assume

$$N_i(\omega) > 0 , \quad \omega \in \mathbb{R}^n , \quad i = 1,2,\ldots,m . \tag{17}$$

We can visualize (17) as is shown in Figure 3*b*. The case of strongly coprime multiple operators has the useful feature that the consideration of (16) and (17) pointwise in conjuction with (8) and (9) uniquely determines an alternative choice for the D_i of (6).

Proposition. For $N_i \in L^\infty(\mathbb{R}^n)$, $N_i(\omega) > 0$ for $\omega \in \mathbb{R}^n$, $i = 1,2,\ldots,m$, then $D : \mathbb{R}^n \longrightarrow \mathbb{C}^m$ is uniquely determined (almost everywhere) by the conditions, for fixed $\omega \in \mathbb{R}^n$,

$$D(\omega) = (D_1(\omega), D_2(\omega),\ldots,D_m(\omega)) = z$$

where

$$z \text{ minimizes } \sum_{i=1}^{m} |z_i|^2 N_i^2(\omega) \quad \text{on the set} \quad \left\{ z \in \mathbb{C}^m : \sum_{i=1}^{m} z_i \hat{\mu}_i(\omega) = 1 \right\} . \tag{18}$$

In fact

$$D_i(\omega) = \frac{\dfrac{\overline{\hat{\mu}}_i(\omega)}{N_i^2(\omega)}}{\displaystyle\sum_{i=1}^{m} \frac{|\hat{\mu}_j(\omega)|^2}{N_i^2(\omega)}} \tag{19}$$

proof: Any z that satisfies (18) is clearly contained in the linear subspace of $\mathbb{C}^n$ determined by the span of

$$\left\{ (\hat{\mu}_1(\omega),0,\ldots,0), \ (0,\hat{\mu}_2(\omega),0,\ldots,0),\ldots, \ (0,0,\ldots 0,\hat{\mu}_m(\omega)) \right\} . \tag{20}$$

That is, $z_i = 0$ if $\hat{\mu}_i(\omega) = 0$. Equivalently, there exists $\lambda = (\lambda_1, \lambda_2,\ldots,\lambda_m) \in \mathbb{C}^m$ such that

$$\left(z_1 N_1(\omega),\ z_2 N_2(\omega), \ldots, z_m N_m(\omega)\right) = \left(\lambda_1 \overline{\hat{\mu}}_1(\omega),\ \lambda_2 \overline{\hat{\mu}}_2(\omega), \ldots, \lambda_m \overline{\hat{\mu}}_m(\omega)\right) . \quad (21)$$

Let $\sum_i'$ denote $\sum_{\substack{i=1 \\ \hat{\mu}_i(\omega) \neq 0}}^{m}$. Then (18) implies

$$\text{minimize} \quad \sum_i' |\lambda_i|^2 |\hat{\mu}_i(\omega)|^2 \quad \text{on} \quad \left\{ \sum_i' \lambda_i \frac{|\hat{\mu}_i(\omega)|^2}{N_i(\omega)} = 1 \right\} . \quad (22)$$

From this it follows that the λ_i are all real, so that (22) in the form

$$\text{minimize} \quad \sum_i' \left(\lambda_i |\hat{\mu}_i(\omega)|\right)^2 \quad \text{on} \quad \left\{ \sum_i' \lambda_i |\hat{\mu}_i(\omega)| \frac{|\hat{\mu}_i(\omega)|}{N_i(\omega)} = 1 \right\} \quad (23)$$

is an elementary case for $\mathbb{R}^n$ and has the unique solution

$$\lambda_i |\hat{\mu}_i(\omega)| = \frac{\dfrac{|\hat{\mu}_i(\omega)|}{N_i(\omega)}}{\displaystyle\sum_{j=1}^{m} \frac{|\hat{\mu}_j(\omega)|^2}{N_j^2(\omega)}} \quad (\text{for } \hat{\mu}_i(\omega) \neq 0) . \quad (24)$$

Consequently, from (21), the unique z corresponding to the minimum is $D(\omega)$ as in (19).

■

In addition to $N_i > 0$, $i = 1,2,\ldots,m$, we shall assume $N_0 > 0$. Further, we shall assume that the N_i are sufficiently differentiable and that $\frac{1}{N_i} = \mathcal{O}(|\omega|^p)$ for some integer p, $i = 0,1,2,\ldots,m$. With this we can find $\hat{\phi} = \mathcal{O}(|\omega|^{p'})$ so that $(D_i \hat{\phi})^\vee \in L^2(\mathbb{R}^n)$ and for $\hat{\phi}$ sufficiently smooth and with compact support then $(D_i \hat{\phi})^\vee \in L^1(\mathbb{R}^n)$.

Corollary. For the choice of D_i from the Proposition,

$$\sum_{i=1}^{m} \hat{\mu}_i D_i = 1 \quad , \quad \left(\sum_{i=1}^{m} |D_i|^2 N_i^2 \right)^{1/2} = \left(\frac{1}{\sum_{j=1}^{m} \frac{|\hat{\mu}_j|^2}{N_j^2}} \right)^{1/2} . \qquad (25)$$

Let L_0 identify the trivial configuration of L in (10) and let L_s identify the strongly coprime configuration. Unless explicitly indicated to the contrary, L_s indicates that the deconvolvers D_i of (19) are used. The first of the functions in (25) is the transfer function for L_s and the second is the square root of the noise power spectral density. The corresponding functions for L_0 are (15). The mollifier $\hat{\phi}$ is suppressed but understood. From (25) obviously $L_s | L$ for any operator L. From (15) and (25) the divisor $\hat{m}$ for $L = L_0$ is $m\hat{\mu}_0$. Let N_s^2 denote the noise power spectral density of L_s. The linear operator associated with $m\hat{\mu}_0$ acting on L_s has functions corresponding to (25) given by

$$m\hat{\mu}_0 \sum_{i=1}^{m} \hat{\mu}_i D_i = m\hat{\mu}_0 \quad ,$$

$$|m\hat{\mu}_0|_{N_s} = m|\hat{\mu}_0| \left(\sum_{i=1}^{m} |D_i|^2 N_i^2 \right)^{1/2} = \left(\frac{m \frac{|\hat{\mu}_0|^2}{N_0^2}}{\sum_{j=1}^{m} \frac{|\hat{\mu}_j|^2}{N_j^2}} \right)^{1/2} \sqrt{m} N_0 \qquad (26)$$

From (15) and (26)

$$|m\hat{\mu}_0|_{N_s}(\omega) \begin{matrix} \leq \\ \geq \end{matrix} \sqrt{m} N_0(\omega) \iff \left(\sum_{i=1}^{m} \frac{N_0^2(\omega)}{N_i^2(\omega)} |\hat{\mu}_i(\omega)|^2 \right)^{1/2} \begin{matrix} \geq \\ \leq \end{matrix} \sqrt{m} |\hat{\mu}_0(\omega)| \quad . (27)$$

The comparison in (27) can in special cases be viewed from a slightly different perspective. First, view the left side of the second inequality in

(27) as the Fourier transform of a kernel. Define

$$\hat{e}(\omega) = \left[\sum_{i=1}^{m} \frac{N_0^2(\omega)}{N_i^2(\omega)} \, |\hat{\mu}_i(\omega)|^2 \right]^{1/2} . \tag{28}$$

We refer to $\hat{e}$ as the *envelope* transfer function corresponding to the *envelope operator* $\mathcal{E}$ for a given strongly coprime L_s in comparison with a given L_0. If $\sqrt{m}\mathcal{E}$ acts on L_s then the pair of functions in (25) becomes

$$\sqrt{m}\,\hat{e} \quad , \quad \sqrt{m}\,N_0 . \tag{29}$$

Recall that the pair for L_0 is (15) (rewritten for convenience)

$$m\,\hat{\mu}_0 \text{ and } \sqrt{m}\,N_0 . \tag{15}$$

If, for example, $\hat{\mu}_0$ is real and positive, then it makes sense to compare (29) with (15) and this comparison leads again to (27). Viewed in this manner, $\sqrt{m}\mathcal{E}$ is the normalization of L_s to the noise power spectral density of L_0.

For either point of view, we consider $W_> = \left\{\omega \in \mathbb{R}^n : \hat{e}(\omega) \geq \sqrt{m}\,|\hat{\mu}_0(\omega)|\right\}$ and $W_< = \left\{\omega \in \mathbb{R}^n : \hat{e}(\omega) \leq \sqrt{m}\,|\hat{\mu}_0(\omega)|\right\}$. For all U such that $\hat{u}$ has support in $W_>$ it follows from (27) and the definitions that $UL_s \geq UL_0$. Consequently,

$$\frac{\mathcal{PNR}(U\mathbb{M}_0 L_s)}{\mathcal{PNR}(UL_0)} = \frac{\left\| \hat{u}\,\hat{\phi}\,N_0 \right\|_2}{\left\| \hat{u}\,\frac{\sqrt{m}\,\hat{\mu}_0}{\hat{e}}\,\hat{\phi}\,N_0 \right\|_2} \geq 1 , \tag{30}$$

where $\mathbb{M}_0$ is used to denote the linear operator corresponding to the transfer function $m\hat{\mu}_0$ of L_0.

Assume $\hat{\mu}_0(0) \neq 0$ and define

$$\Omega_0 = \{\, \omega \in \mathbb{R}^n : \forall t \in [0,1) \;\; |\hat{\mu}_0(t\omega)| > 0 \,\} .$$

Note that for $\mathbb{R}^1$ the usual definition of limiting resolution is sup Ω_0. If supp$(\hat{u})$ is compact and supp$(\hat{u}) \subset \Omega_0$, then $U\mathbb{M}_0^{-1}$ makes sense, consequently

$uL_0 \,|\, uL_s$. Hence, if $\mathrm{supp}(\hat{u})$ is compact and $\mathrm{supp}(\hat{u}) \subset W_< \cap \Omega_0$, then $uL_0 \geq uL_s$. Consequently,

$$\frac{\mathcal{PNR}(uL_s)}{\mathcal{PNR}(u\mathbb{m}_0^{-1}L_0)} = \frac{\left\| \hat{u}\ \frac{1}{\sqrt{m}\ \hat{\mu}_0}\ \hat{\phi}\ N_0 \right\|_2}{\left\| \hat{u}\ \frac{1}{\hat{e}}\ \hat{\phi}\ N_0 \right\|_2} \leq 1 \ . \tag{31}$$

In general the inequality cannot be extended to all of $W_< \cap \Omega_0$ because of the behavior of $1/\hat{\mu}_0$ on the boundary.

There is no information regarding $\dfrac{\mathcal{PNR}(uL_s)}{\mathcal{PNR}(uL_0)}$ implied by either $uL_s \geq uL_0$ or $uL_s \geq uL_0$. Additional information is needed. For example, it may be sufficient to know the effect of the so-called "boost" $uL_0 \longmapsto u\mathbb{m}_0^{-1}L_0$. In particular, if $\mathrm{supp}(\hat{u})$ is compact and $\mathrm{supp}(\hat{u}) \subset \Omega_0$ then

$$\mathrm{supp}(\hat{u}) \subset W_> \quad \text{and} \quad \frac{\mathcal{PNR}(u\mathbb{m}_0^{-1}L_0)}{\mathcal{PNR}(uL_0)} \geq 1 \quad \Longrightarrow \quad \frac{\mathcal{PNR}(uL_s)}{\mathcal{PNR}(uL_0)} \geq 1 \ , \tag{32a}$$

and

$$\mathrm{supp}(\hat{u}) \subset W_< \quad \text{and} \quad \frac{\mathcal{PNR}(u\mathbb{m}_0^{-1}L_0)}{\mathcal{PNR}(uL_0)} \leq 1 \quad \Longrightarrow \quad \frac{\mathcal{PNR}(uL_s)}{\mathcal{PNR}(uL_0)} \leq 1 \ . \tag{32b}$$

For $\mathrm{supp}(\hat{u}) \subset \mathbb{R}^n - \Omega_0$ it is often the case in applications that uL_0 is not defined. Since uL_s is defined for all u it makes sense in such cases to consider $uL_s \geq uL_0$.

EXAMPLES: CHARACTERISTIC FUNCTIONS OF SETS IN $\mathbb{R}^n$

Collections of sets in $\mathbb{R}^n$ such that the characteristic functions of the sets in the collection are strongly coprime have been reported [5,6,10]. For example, such a collection of cubes consists of m = n+1 cubes in $\mathbb{R}^n$ with sides parallel and with side lengths $\sqrt{a_1}$, $\sqrt{a_2}$,..., $\sqrt{a_m}$, where for all $i \neq j$ a_i and a_j are relatively prime integers and for all i $\sqrt{a_i}$ is not an integer. A second example is the collection of m = 2 disks in $\mathbb{R}^n$ with the ratio of the radii of the form p/q, where p and q are distinct integers between 1 and 200.

A common situation for electro-optic detectors on $\mathbb{R}^n$ (e.g., n=1 (slits), n=2 (focal plane arrays), n=3 ($\mathbb{R}^2 \times \{\text{time}\}$)) is for the noise power spectral density to have the form $\|\chi_S\|_1 N_\emptyset^2$, where $\|\chi_S\|_1$ is the L^1 norm of the characteristic function χ_S of the set S (equivalently, the Lebesgue measure of the set). For such a case, let sets S_1, S_2,..., S_m, be chosen so that, for $\mu_i = \chi_{S_i}$, the μ_1, μ_2,...,μ_m are strongly coprime. Then, from the Proposition,

$$D_i(\omega) = \frac{\dfrac{\overline{\hat{\mu}}_i(\omega)}{\|\mu_i\|_1}}{\displaystyle\sum_{i=1}^{m} \frac{|\hat{\mu}_j(\omega)|^2}{\|\mu_j\|_1}} \tag{33}$$

and (25) becomes

$$\sum_{i=1}^{m} \hat{\mu}_i D_i = 1 \quad , \quad \left(\sum_{i=1}^{m} |D_i|^2 N_i^2 \right)^{1/2} = \left(\frac{1}{\displaystyle\sum_{j=1}^{m} \frac{|\hat{\mu}_j|^2}{\|\mu_j\|_1}} \right)^{1/2} N_\emptyset \quad . \tag{34}$$

Let S_0 be any set, let $\mu_0 = \chi_{S_0}$ be its characteristic function, and consider this to be the convolver in L_0 defined by (10) (i.e., m parallel, identical

convolvers). Let the noise power spectral density have the same form as above, $N_0^2 = \|\mu_0\|_1 N_\emptyset^2$. From (27) and (28) one obtains an envelop transfer function $\hat{e}_d$ and the associated comparison for these two: a convenient renormalization by the constant $\|\mu_0\|_1^{1/2}$ is made in

$$\hat{e}_d(\omega) = \frac{\hat{e}(\omega)}{\|\mu_0\|_1^{1/2}} = \left[\sum_{i=1}^{m} \frac{|\hat{\mu}_i(\omega)|^2}{\|\mu_i\|_1} \right]^{1/2} \begin{matrix} \geq \\ \leq \end{matrix} \sqrt{m}\, \frac{|\hat{\mu}_0(\omega)|}{\|\mu_0\|_1^{1/2}} . \qquad (35)$$

For an explicit example let $S_i \subset \mathbb{R}^2$ be the region in a focal plane of an imaging device which corresponds to a single light sensitive detector. The exposure time interval is assumed fixed and the image is assumed constant. Then $\mu_i = \chi_{S_i}$ is the idealized response function of the detector. (The consequence of the actual shape of the response function is considered later.) Then $\hat{\mu}_i$ is what is referred to as the "detector MTF" and the form of the noise power spectral density corresponds to typical detector properties such as "D^*" for infrared detectors. The density has the above form as well for the so-called background limited case. It also has this form for $\mathbb{R}^3$ when the time interval is included as the third dimension. Further, a background limited slit detector corresponds to the above forms for $\mathbb{R}^1$ with the slit width as the coordinate. (In the background limited case there is assumed to be a relatively small signal of interest superimposed on a relatively large constant signal so that the noise in the signal of interest is due to the "shot" noise of the constant signal.)

In Figures 4 and 5 the transfer functions for such cases are shown. In Figure 4, a comparison is shown for the example for $\mathbb{R}^1$. The characteristic functions μ_1 and μ_2 for the two intervals $\left(-\frac{1}{2}, \frac{1}{2}\right)$ and $\left(-\frac{\sqrt{2}}{2}, \frac{\sqrt{2}}{2}\right)$, respectively, are strongly coprime. The envelope transfer function $\hat{e}_d$ is shown

and is compared with the transfer function for the two identical, parallel convolvers as in (35) where $\mu_0 = \mu_1$. This illustrates the consequence of the strongly coprime condition: the envelope response is approximately an envelope for the modulus of the other two responses and, correspondingly, is without zeroes. Also, it can be observed that the envelope response decreases approxiamately as $1/|\omega|$.

In Figure 5 the envelope transfer function is shown for an example in $\mathbb{R}^2$, the case of three cubes (squares) Q_1, Q_2, Q_3 of side length 1, $\sqrt{2}$, $\sqrt{3}$, respectively. The characteristic functions of these three cubes are strongly coprime. The comparison (35) is illustrated by graphing the modulus of the corresponding transfer functions for two subsets of $\mathbb{R}^2$: the ω_1-axis $\left\{\omega=(\omega_1,\omega_2) \in \mathbb{R}^2 : \omega_2=0\right\}$ and the diagonal $\left\{\omega=(\omega_1,\omega_2) \in \mathbb{R}^2 : \omega_1=\omega_2\right\}$. All graphs use the Euclidean distance as abscissa, $|\omega| = \left(\omega_1^2 + \omega_2^2\right)^{1/2}$. The comparison illustrated in Figure 5 is for $\hat{\mu}_0 = \hat{\chi}_{Q_1}$. The comparison is essentially the same as that for the two intervals in $\mathbb{R}^1$. The difference between the ω_1-axis and the diagonal illustrates that approximately the envelope response decreases as $|\omega|^{-1}$ along the ω_1-axis and as $|\omega|^{-2}$ along the diagonal.

From (35) (and as illustrated by the figures) the following statements can be made. These are stated as "observations" because the results can not be given in terms of explicit inequalities. Some notation is helpful. Define

$$\Omega_i = \{\ \omega \in \mathbb{R}^n : \forall t \in [0,1)\ \ |\mu_i(t\omega)| > 0\ \} \quad \text{and} \quad \Omega = \bigcap_{i=1}^{m} \Omega_i \ . \tag{36}$$

Observations: Let $\mu_1, \mu_2, \ldots, \mu_m \in L^1(\mathbb{R}^n)$ be strongly coprime characteristic functions of sets in $\mathbb{R}^n$ as considered above. With each μ_i let there be

associated as in Figure 2 an additive wide sense stationary noise with noise power spectral density of the form $\|\mu_i\|_1 N_\emptyset^2$. Let L_s be the configuration in Figure 2 with deconvolvers determined by the Proposition. Let L_0 be the trivial configuration as in (10) with $\mu_0 = \mu_1$, $N_0 = N_1$.

Observation 1: For u with $\text{supp}(\hat{u}) \subset \Omega$ $uL_s \cong uL_0$.

Observation 2: For u with $\text{supp}(\hat{u}) \subset \mathbb{R}^n - \bigcup_{i=2}^{m} \Omega_i$, $uL_s \geq uL_0$.

Observation 3: For u with $\text{supp}(\hat{u}) \subset \bigcup_{i=2}^{m} \Omega_i - \Omega$, $uL_s \leq uL_0$.

Observation 4: For u with $\text{supp}(\hat{u})$ compact, $\text{supp}(\hat{u}) \subset \Omega_1$, let $\mathbb{M}_0^{-1}$ be the boost on u $uL_0 \longmapsto u\mathbb{M}_0^{-1}L_0$ (see (31) and (32)). If *Observation 3* can be neglected then

$$\frac{\mathcal{PNR}(u\mathbb{M}_0^{-1}L_0)}{\mathcal{PNR}(uL_0)} \geq 1 \quad \Longrightarrow \quad \frac{\mathcal{PNR}(uL_s)}{\mathcal{PNR}(uL_0)} \geq 1 \quad .$$

As discussed at (31) it is not possible to extend this to all of Ω_1, for $\hat{\mu}_1 = 0$ on the boundary of Ω_1. However, it still is desirable to have a means to compare L_s with the more well known, more thoroughly studied trivial configurations. In the next section this is accomplished by pushing the troublesome set $\{\hat{\mu}_1 = 0\}$ out toward infinity.

An explicit example

It is instructive to consider $\dfrac{\mathcal{PNR}(uL_s)}{\mathcal{PNR}(uL_0)}$ for some explicit choices for $N_\emptyset$, f, u, and for $\mathcal{P}$. Let $N_\emptyset$ be the constant function. For fixed $\omega_0 \in \mathbb{R}^n$, let $f(x) = 1 + \exp(i\omega_0 \cdot x)$, $x \in \mathbb{R}^n$. Let $\mathcal{P}u(E\{g\}) = \left|\left(u(E\{g\})\right)(0)\right|$, and let $\hat{u} = \hat{u}_\ell$ be the characteristic function of the punctured (excludes $\omega = 0$) closed disk centered at the origin and of radius L, $|\omega_0| < \ell$. (Alternaltively, the

punctured cube of side lenght 2ℓ, or the set $\left\{\omega\in\mathbb{R}^n : |\omega_i| \le \ell_i, i=1,2,\ldots,n\right\}$. This later alternative, $\hat{u}_\ell$ the characteristic function of the set $\left\{\omega \in \mathbb{R}^2 : |\omega_1| \le 2|\omega_0|, |\omega_2| \le \frac{2}{5}|\omega_0|\right\}$, with $f(x) = 1 + \exp\left[ix_1(\omega_0)_1\right]$, is a very coarse approximation of a standard vision model [11].) Then from (14), (34), and (35), with C a constant,

$$\mathcal{PNR}(uL_s) = C\,\frac{|\hat{\phi}(\omega_0)\hat{f}(\omega_0)|}{\left\| \dfrac{\hat{\phi}\ \hat{u}\ N_\emptyset}{\hat{e}_d} \right\|_2} \qquad \mathcal{PNR}(uL_0) = C\,\frac{|\hat{\phi}(\omega_0)\ \sqrt{m}\ \hat{\mu}_1(\omega_0)\ \hat{f}(\omega_0)|}{\|\mu_1\|_1^{1/2}\ \|\hat{\phi}\ \hat{u}\ N_\emptyset\|_2}$$

hence

$$\frac{\mathcal{PNR}(uL_s)}{\mathcal{PNR}(uL_0)} = \frac{\|\hat{\phi}\ \hat{u}\ N_\emptyset\|_2}{\dfrac{\sqrt{m}\,|\hat{\mu}_1(\omega_0)|}{\|\mu_1\|_1^{1/2}} \left\| \dfrac{\hat{\phi}\ \hat{u}\ N_\emptyset}{\hat{e}_d} \right\|_2}. \tag{37}$$

For the examples above, with $\mathcal{D}(\omega) = \dfrac{\sqrt{m}\,|\hat{\mu}_1(\omega_0)|}{\|\mu_1\|_1^{1/2}} \dfrac{1}{\hat{e}_d(\omega)}$, for $\omega\in\Omega_1$,

$$\mathcal{D}(\omega_0) \cong 1, \qquad \mathcal{D}(\omega) \le 1 \text{ for } |\omega| \le |\omega_0|, \qquad \text{and } \mathcal{D}(\omega) \ge 1 \text{ for } |\omega| \ge |\omega_0|.$$

Qualitatively

$$\frac{\mathcal{PNR}(uL_s)}{\mathcal{PNR}(uL_0)} \ge 1 \text{ for } \ell = |\omega_0|, \text{and } \frac{\mathcal{PNR}(uL_s)}{\mathcal{PNR}(uL_0)} \le 1 \text{ for } \ell = |\omega_0| + \Delta \text{ and for } \Delta$$

sufficiently large. This example highlights the difference between the two independent statements $uL_s \ge uL_0$ and $\mathcal{PNR}(uL_s) \ge \mathcal{PNR}(uL_0)$.

The elementary $\mathfrak{P}$ makes this example a candidate for the use of $\hat{e}_d$ as the transfer function of an operator in order to normalized L_s to have the same noise power spectral density as L_0, as was mentioned at (29). Let $\mathfrak{E}_d$ denote this linear operator. Then, proceeding exactly as for (37)

$$\frac{\mathcal{PNR}(U\mathcal{E}_d L_s)}{\mathcal{PNR}(UL_0)} = \frac{\hat{e}_d(\omega_0)}{\frac{\sqrt{m}\,|\hat{\mu}_1(\omega_0)|}{\|\mu_1\|_1^{1/2}}} \quad , \ \omega_0 \in \Omega_1 \ . \tag{38}$$

For the cases considered this is approximately unity except for ω_0 near the zero set of $\hat{\mu}_1$. The significance of (38) is that it is an explicit example of Observations 1 and 2: on Ω_1 L_s is at least as good as L_0 with the additional feature of extended frequency response outside of Ω_1. That is, on Ω_1 there is no penalty for the additional response outside of Ω_1. On the other hand, (38) only gives essentially equivalent performance on Ω_1, despite the fact that $\hat{e}_d$ has no zeroes. Once again, any advantage due to this later depends on

$$\sup_{\mathcal{B}} \frac{\mathcal{PNR}(U\mathcal{B}\mathcal{E}_d L_s)}{\mathcal{PNR}(U\mathcal{E}_d L_s)} = \sup_{\hat{b}} \frac{\| \hat{\phi}\,\hat{u}\,N_\emptyset \|_2}{\left\| \frac{\hat{\phi}\,\hat{u}\,\hat{b}\,N_\emptyset}{\hat{b}(\omega_0)} \right\|_2} \ , \tag{39}$$

where $\mathcal{B}$ is a linear operator and $\hat{b}$ its transfer function. It is clearly possible for $\mathcal{E}_d L_s$ to be the optimal: for example, consider $\hat{\phi}\hat{u}N_\emptyset$ constant and $\hat{b}$ convex.

This consideration is of significance for operators $\mu_1, \mu_2, \ldots, \mu_m$ that are not characteristic functions of sets but rather have each $\hat{\mu}_i$ approximately compactly supported. The primary example here is the diffraction limited lens. If strongly coprime convolvers $\mu_1, \mu_2, \ldots, \mu_m$ were such that each $|\hat{\mu}_i|$ was small outside some set, then the envelope transfer function would exhibit the same behavior. In this case, unless $\sup_{\mathcal{B}} \mathcal{PNR}(U\mathcal{B}\mathcal{E}L_s)$ is substantially greater than $\mathcal{PNR}(U\mathcal{E}L_s)$, the performance of the strongly coprime configuration will be essentially that of its constituent convolvers.

MORE COMPARISONS: STRONGLY COPRIME VERSUS CHANGE OF SCALE

Let L_s be the as above. In the above L_s was compared with L_0, where L_0 was chosen to be μ_1 and $N_1^2 = \|\mu_1\|_1 N_\emptyset^2$. In these cases μ_1 was the "best" in the sense $\Omega_i \subset \Omega_1$ i=1,2,...,m. Here L_s will be compared with a one parameter family of such L. Define L_∂ by the trivial configuration of m parallel, identical $\mu_{\langle\partial\rangle}$ as in (10), where $N_\partial^2 = \|\mu_{\langle\partial\rangle}\|_1 N_\emptyset^2$ and $\mu_{\langle\partial\rangle}(x) = \mu_1\left(\frac{x}{\partial}\right)$, $\partial > 0$.

The primary result of this section is

Oberservation for fixed number of channels: Fix the number of parallel convolvers in both L_s and L_∂ to be m. Let the convolvers be characteristic functions of cubes on $\mathbb{R}^n$ and let the additive noise be as above. Assume that u is such that $\text{supp}(\hat{u}) \subset \bigcup_{j=1}^{m} \left\{\omega \in \mathbb{R}^n : \omega_i = 0,\ i \neq j\right\}$. Then for $n \geq 2$

$$uL_s \geq uL_\partial \qquad \text{for all } 0 < \partial \leq 1 . \tag{40}$$

Corollary to Observation: For the conditions in the Observation above, it is advantageous to construct L_s using sets that are as large as possible.

Application of the Corollary: In parallel scanned imaging systems with square detectors wherein the systems are ranked using some u meeting the conditions of the Observation (e.g., horizontal or vertical bars), the detector size should be sufficiently large so that the array of detectors fills the image, and the detector sizes in the array should constitute a strongly coprime collection. (This application depends on sufficiently high sampling rates. See [ ] .)

The Observation is illustrated in Figure 6 for n = 2. For Figure 6 L_s is as in Figure 5: in the notation just above L_s is configured from the parallel

convolvers $\mu_{\langle 1\rangle}$, $\mu_{\langle\sqrt{2}\rangle}$, $\mu_{\langle\sqrt{3}\rangle}$, and μ_1 is the characteristic function of the unit cube (square). For this L_s the envelope transfer function $\hat{e}_d$ is compared with $\sqrt{3}\,\dfrac{|\hat{\mu}_{\langle\vartheta\rangle}|}{\|\mu_{\langle\vartheta\rangle}\|_1^{1/2}}$, as in (35), for ϑ = 1, 0.5, 0.2, and 0.1 . The observation in (40) is clearly evident. (Here we neglect *Observation 3* of the last section by means of a broad interpretation of $\cong$ in *Observation 1.*)

The Observation (40) depends on the following properties. The first, which is again an approximation, is that for $A_j = \left\{\omega \in \mathbb{R}^n : \omega_i = 0,\ i\neq j\right\}$, the ω_j-axis,

$$\hat{e}_d\,|_{A_j}(\omega) \cong C|\omega|^{-1} . \tag{41}$$

The second is that $\dfrac{|\widehat{\mu_{\langle\vartheta\rangle}}(\omega)|}{\|\mu_{\langle\vartheta\rangle}\|_1^{1/2}} = \vartheta^{n/2}\,\dfrac{|\hat{\mu}_1(\vartheta\omega)|}{\|\mu_1\|_1^{1/2}}$. Hence, for $n \geq 2$,for $\vartheta \leq 1$, and for $\omega \in A_j$, $\sqrt{m}\,\dfrac{|\hat{\mu}_1(\omega)|}{\|\mu_1\|_1^{1/2}} \leq C|\omega|^{-1} \implies \sqrt{m}\,\dfrac{|\widehat{\mu_{\langle\vartheta\rangle}}(\omega)|}{\|\mu_{\langle\vartheta\rangle}\|_1^{1/2}} \leq C|\omega|^{-1}$.

Figures 7 and 8 show two counterexamples for cases not addressed in the Observation. Figure 7 is for the case of the diagonal in $\mathbb{R}^2$, and Figure 8 is for n = 1. The Observation fails on the diagonal $\mathcal{D} = \left\{\omega=(\omega_1,\omega_2) \in \mathbb{R}^2 : \omega_1=\omega_2\right\}$ because

$$\hat{e}_d\,|_{\mathcal{D}}(\omega) \cong C|\omega|^{-2} . \tag{42}$$

It fails for $\mathbb{R}$ because (41) holds.

If in place of characteristic functions of cubes one uses characteristic functions of disks on $\mathbb{R}^2$, then the relationship between $\hat{e}_d$ and $\sqrt{m}\,\dfrac{|\widehat{\mu_{\langle\vartheta\rangle}}|}{\|\mu_{\langle\vartheta\rangle}\|_1^{1/2}}$ is intermediate between that of the ω_j-axis and that of the diagonal for

$$\hat{e}_d(\omega) \cong C|\omega|^{-3/2}. \tag{43}$$

The significance of the Observation (40) is that it provides a qualitative lower bound for the performance of the strongly coprime configuration. To the extend performance is characterized for the uL_{∂}, the "envelope" consisting of the collection over all ∂ is a lower bound for the performance of uL_s.

All of the above has focused on performance away from the origin. If the figures are rescaled so that the $\mu_{<\partial>}$ appear fixed with a sequence of L_s constructed form convolvers of increasing support, the Observation indicates that nothing is sacrificed away from zero while the envelope transfer function near zero is substantially increased. That is, $uL_s \geq uL_{\partial}$ represents a substantial enhancement near $\omega = 0$, not merely approximately identical performance. On the other hand, this uniform improvement is for the case of u supported by the axes. For the cases off the axes for cubes and for the case of disks there is a trade-off between some loss away from zero and the gain near zero.

BIBLIOGRAPHY

[1] J. J. Kelleher and B. A. Taylor, Finitely generated ideals in rings of analytic functions, *Math. ann.* 193 (1971), 225-237.

[2] C. A. Berenstein and B. A. Taylor, A new look at interpolation theory for entire functions of one variable, *Advances in Mathematics* 33 (1979), 109-143.

[3] C. A. Berenstein and B. A. Taylor, Mean periodic functions, *Intern. J. Math. and Math. Sciences* 3 (1980), 199-236.

[4] C. A. Berenstein and B. A. Taylor, Interpolation problems in $\mathbb{C}^n$ with applications to harmonic analysis, *J. Analyse Math.* 38 (1980), 188-254.

[5] C. A. Berenstein, B. A. Taylor, and A. Yger, Sur quelques formules explicites de deconvolution, *Journal of Optics* 14 (1983), 75-82.

[6] C. A. Berenstein, B. A. Taylor, and A. Yger, On some explicit deconvolution formulas, Technical Digest, Signal Recovery, Optical Society of America, Winter Meeting 1983, pages WA4-1 to WA4-4.

[7] C. A. Berenstein and A. Yger, Le probleme de la deconvolution, *J. Funct. Anal.* 54 (1983), 113-160.

[8] C. A. Berenstein, An application of the Andersson-Berndtsson integral representation formula, *Revue de l'Institut Elie Cartan* 8 (1983), 113-160.

[9] C. A. Berenstein, P. S. Krishnaprasad, and B. A. Taylor, Deconvolution methods for multi-sensors, ARO contract DAAG29-81-D0100, DTIC no. AD A152 351, (1984), 68 pages.

[10] E. V. Patrick, Deconvolution for the case of multiple characteristic functions of cubes in $\mathbb{R}^n$, Systems Research Center, Univ. of Maryland, Technical Report, Sept. 1986.

[11] J. A. Ratches, W. R. Lawson, et.al., Night Vision Laboratory static performance model for thermal viewing systems, ECOM Technical Report ECOM-7043, April 1975.

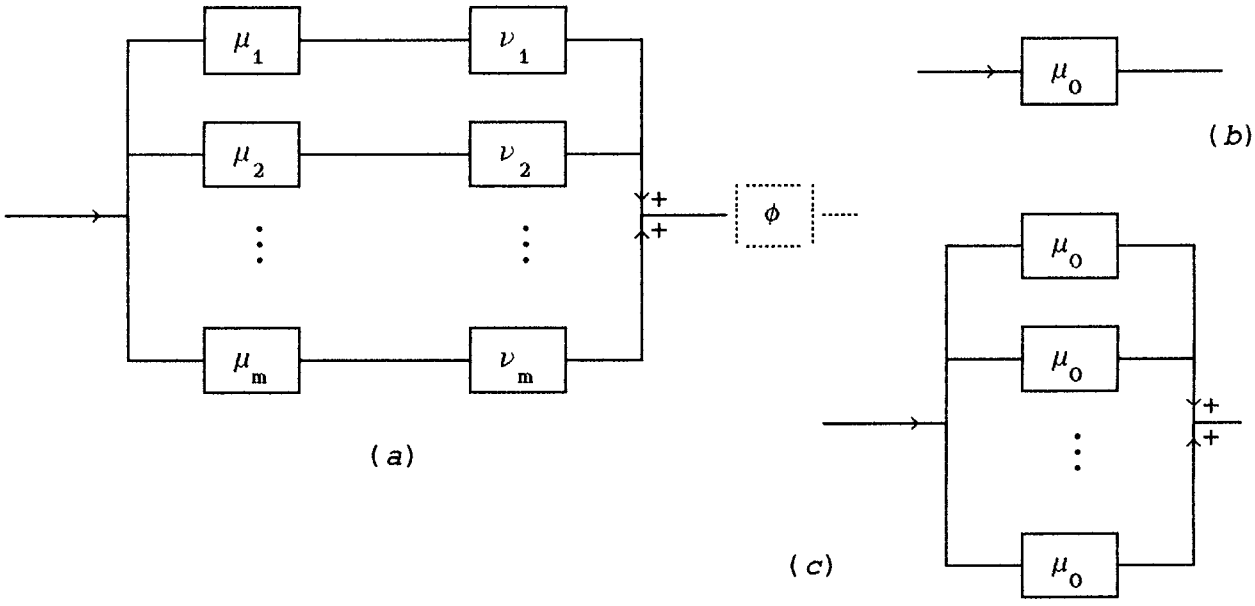

Fig. 1. (*a*) Multiple parallel linear operators with distinct distributions μ_i. Single operator (*b*) and multiple parallel operators with identical distributions μ_0 (*c*).

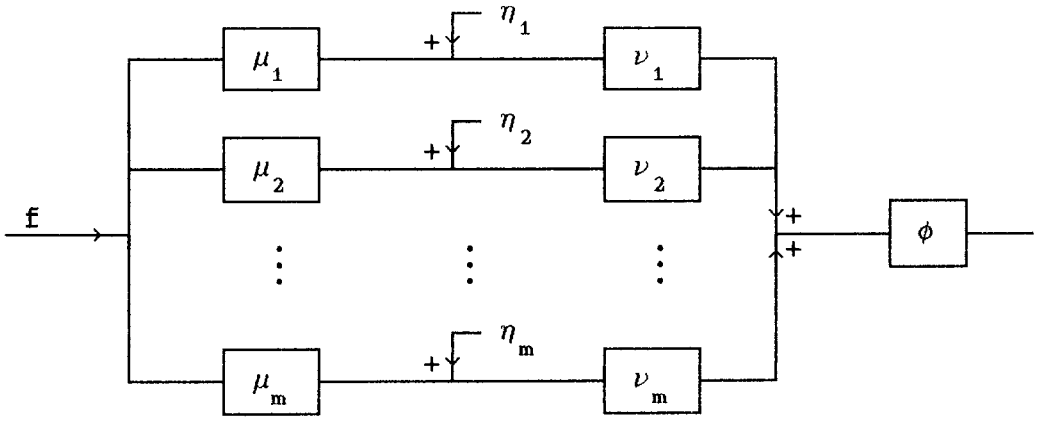

Fig. 2. Multiple operator configuration consisting of m parallel convolvers μ_i, m noise signals η_i, and m deconvolvers ν_i.

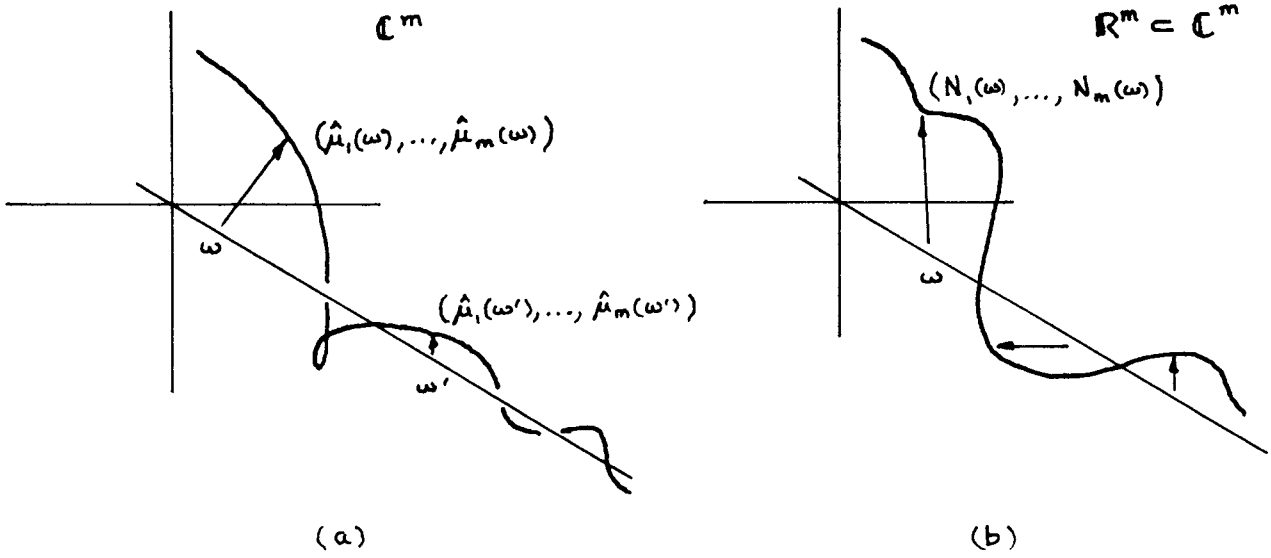
$\mathbb{C}^m$
$(\hat{\mu}_1(\omega), \ldots, \hat{\mu}_m(\omega))$
ω
$(\hat{\mu}_1(\omega'), \ldots, \hat{\mu}_m(\omega'))$
ω'
(a)
$\mathbb{R}^m \subset \mathbb{C}^m$
$(N_1(\omega), \ldots, N_m(\omega))$
ω
(b)

FIG. 3.

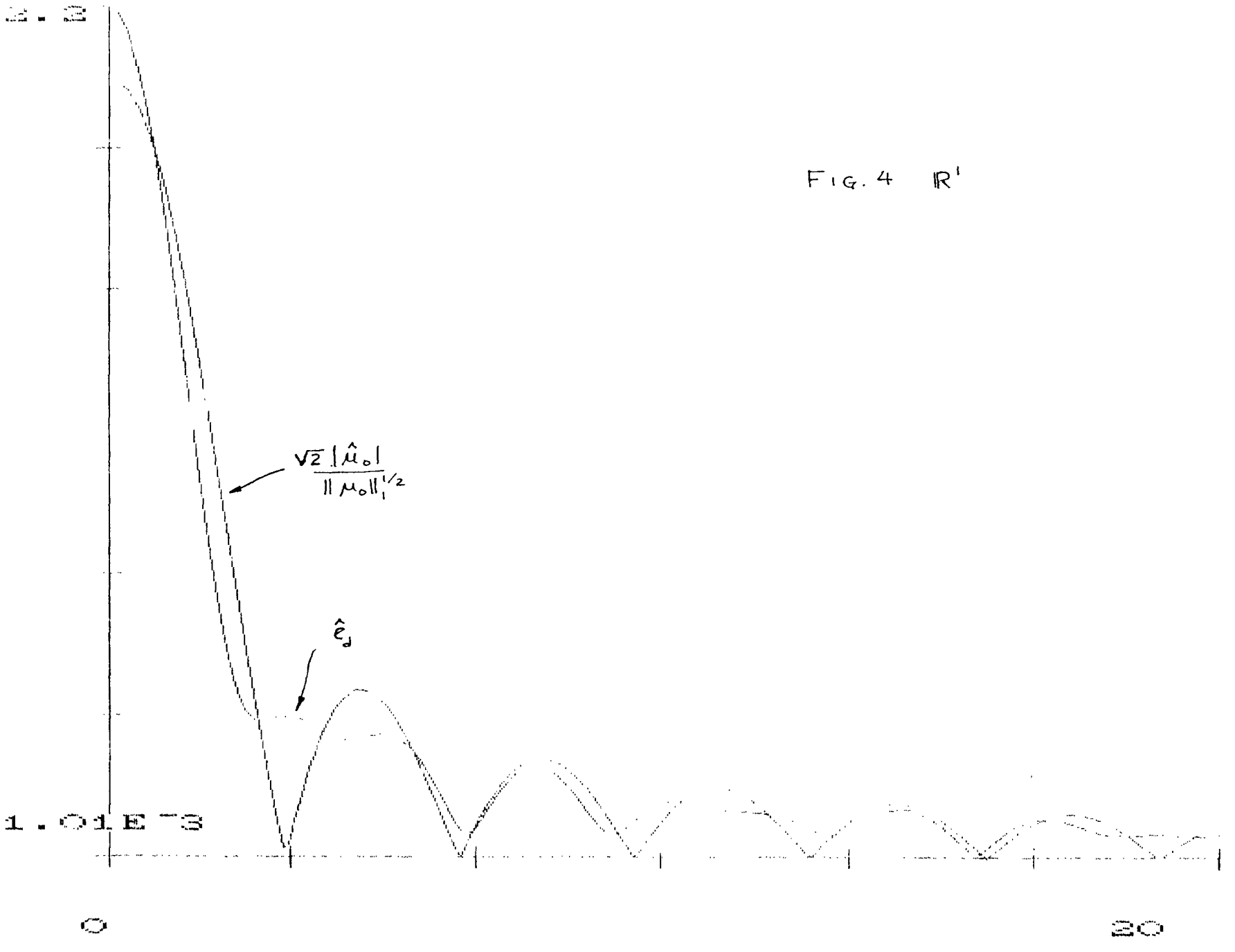

FIG. 4 $\mathbb{R}^1$

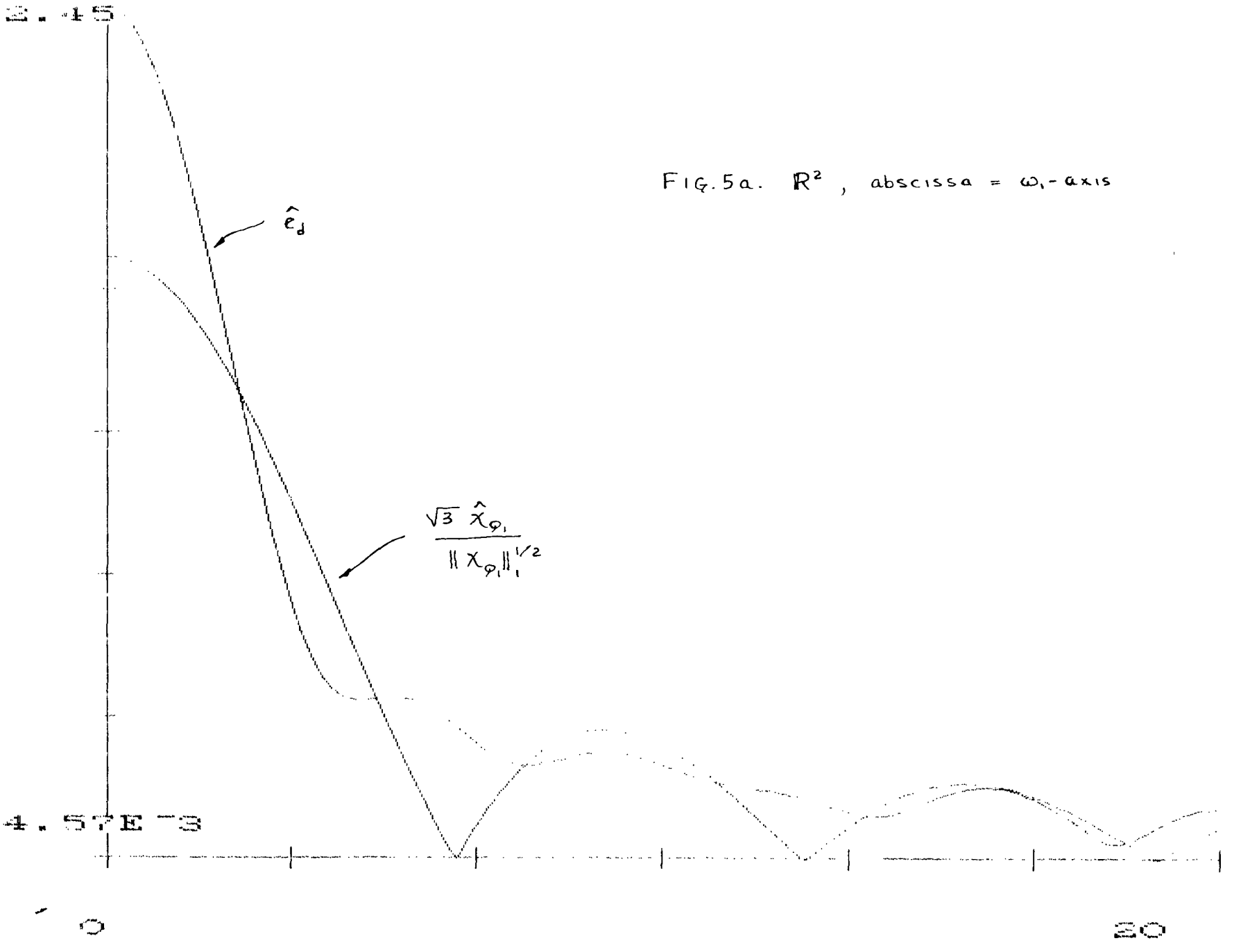

FIG. 5a. $\mathbb{R}^2$, abscissa = ω_1-axis

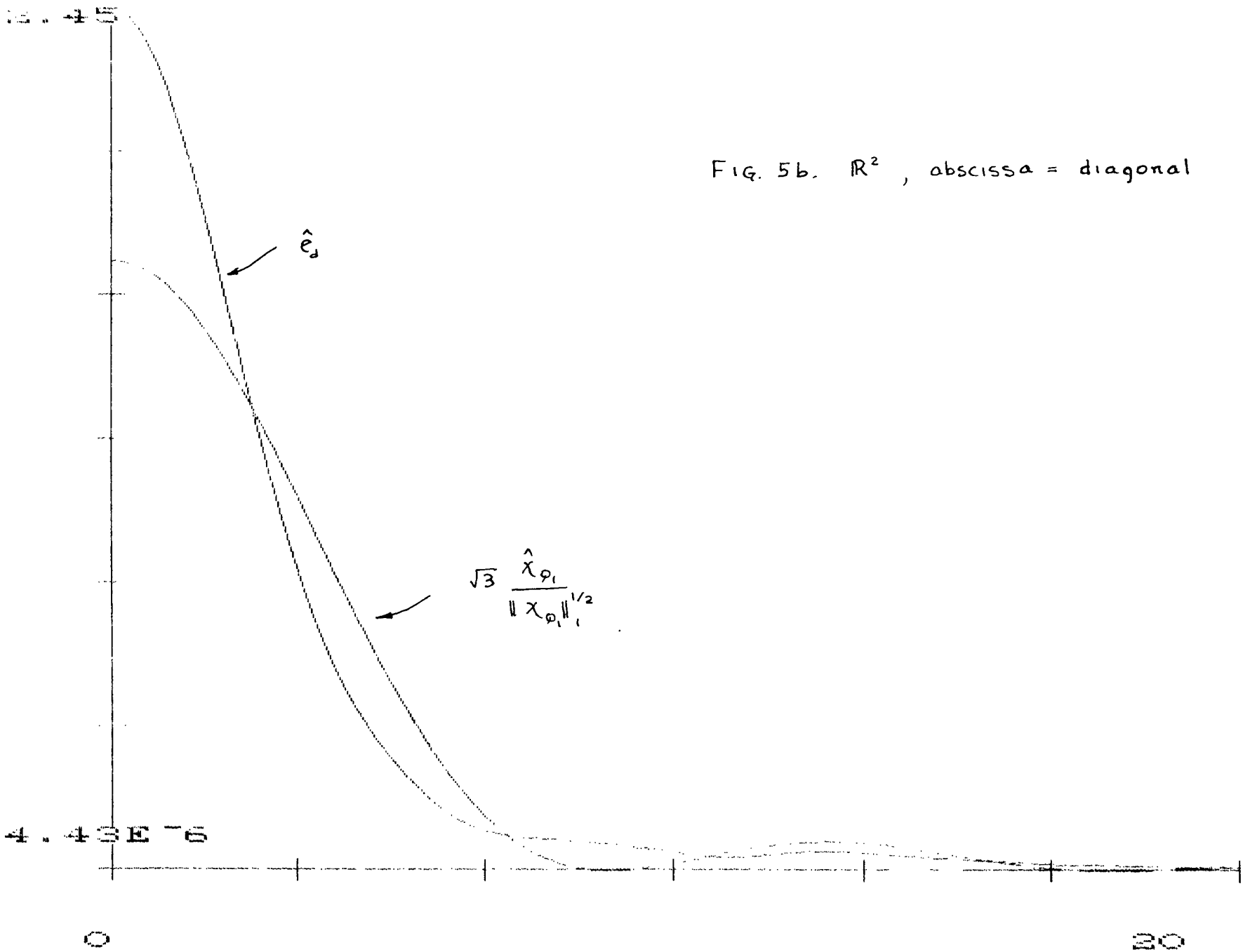

FIG. 5b. $\mathbb{R}^2$, abscissa = diagonal

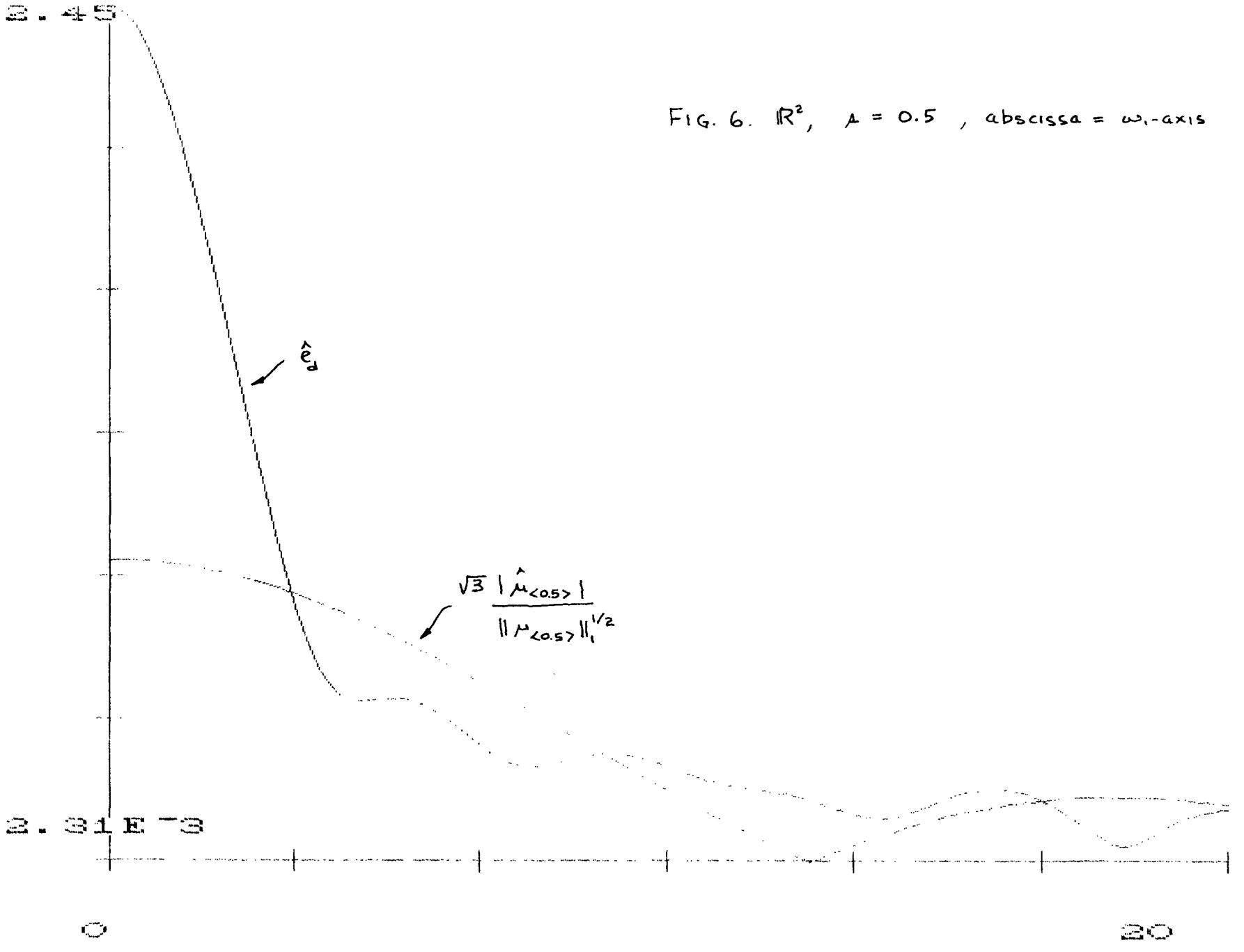

FIG. 6. $\mathbb{R}^2$, $\lambda = 0.5$, abscissa = ω_1-axis

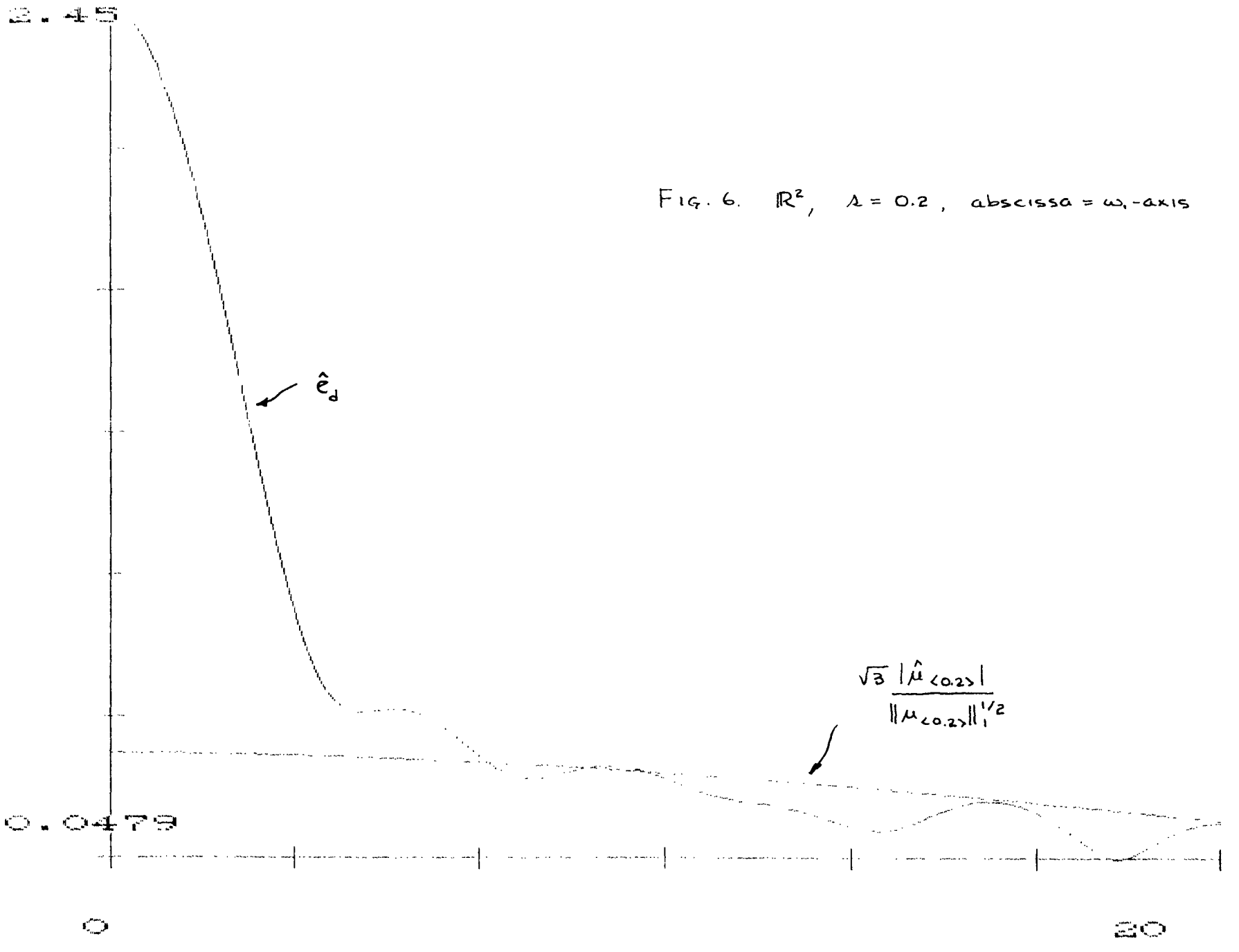

FIG. 6. $\mathbb{R}^2$, $\lambda = 0.2$, abscissa = ω_1-axis

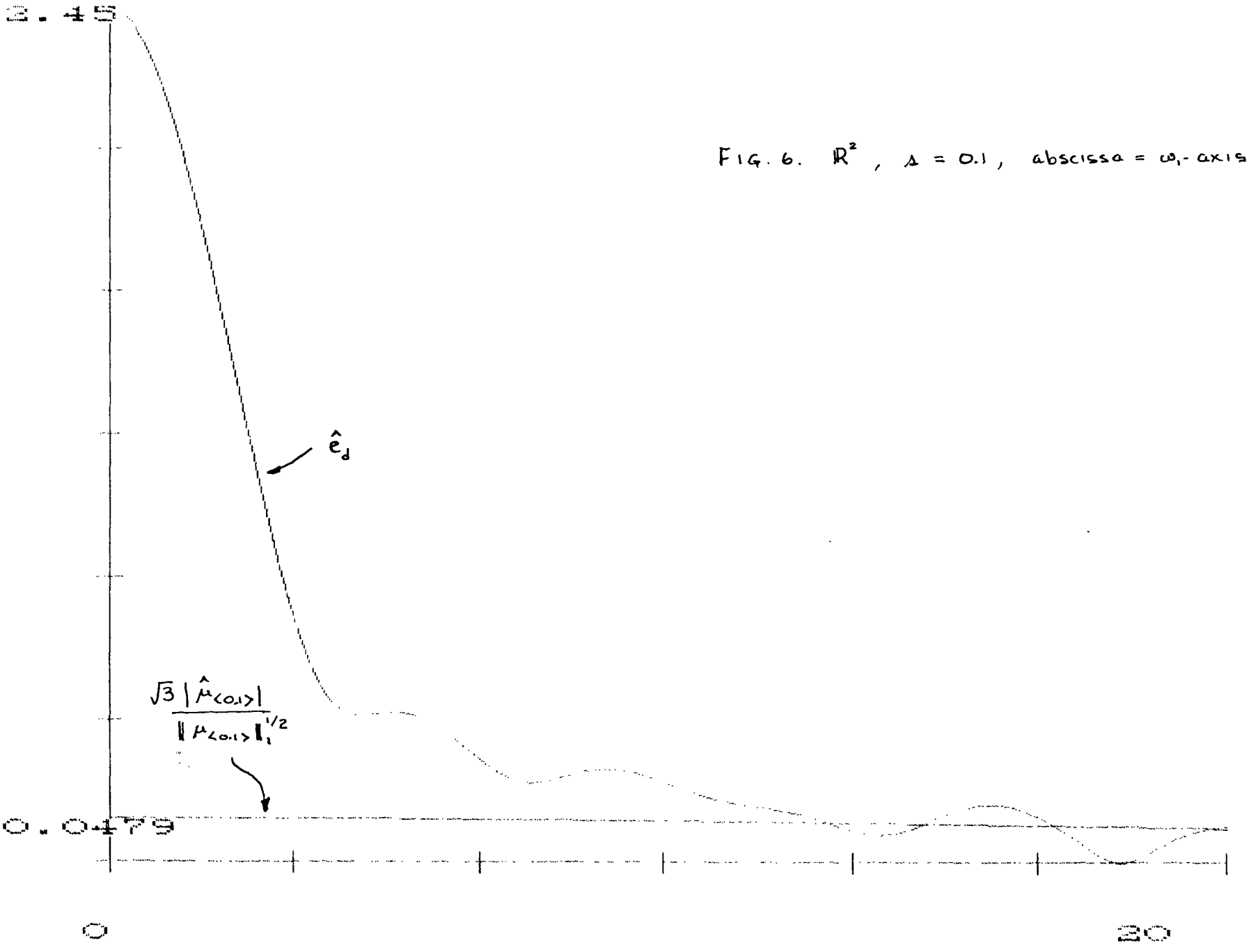

FIG. 6. $\mathbb{R}^2$, $\Delta = 0.1$, abscissa = ω_1-axis

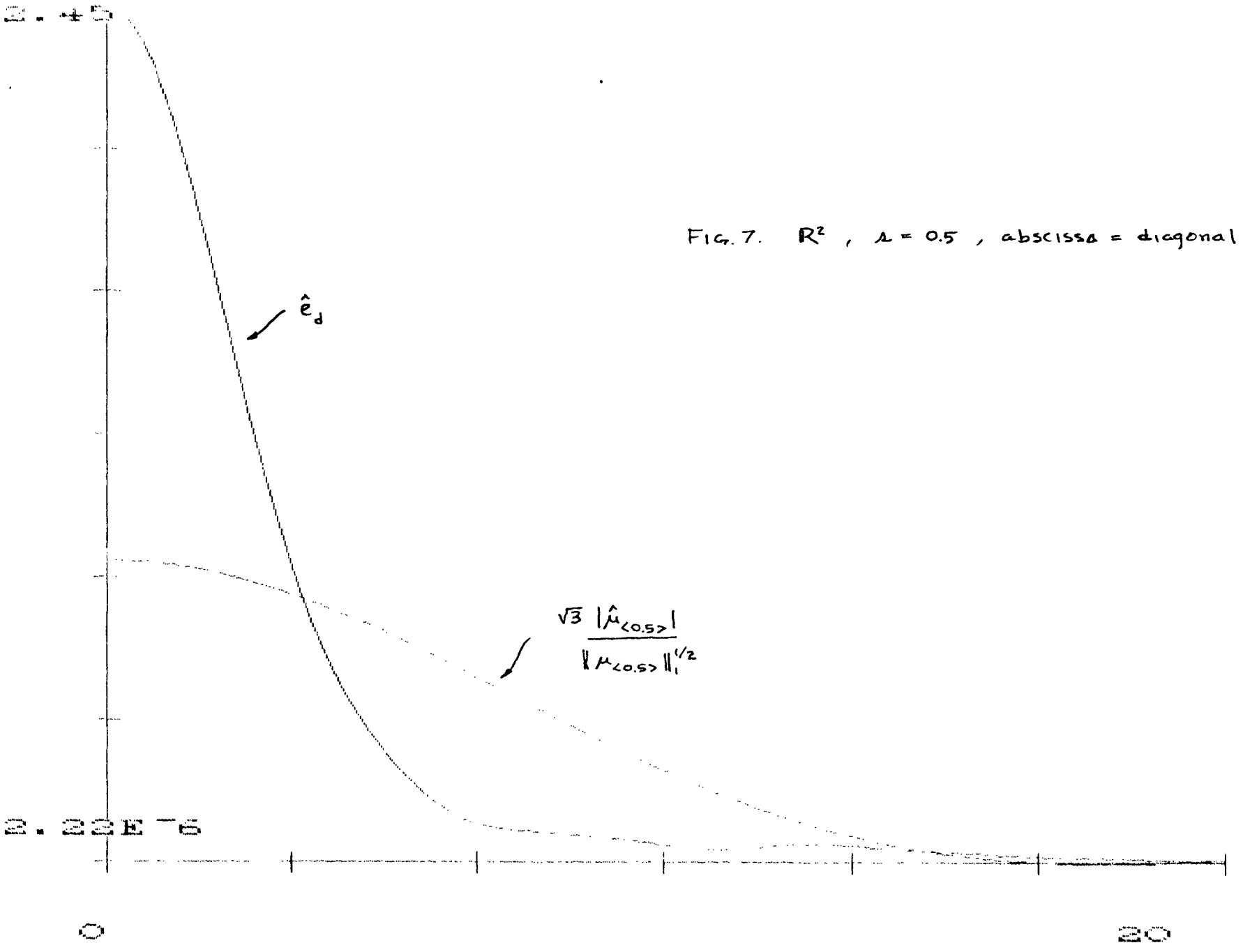

FIG. 7. R^2 , $\alpha = 0.5$, abscissa = diagonal

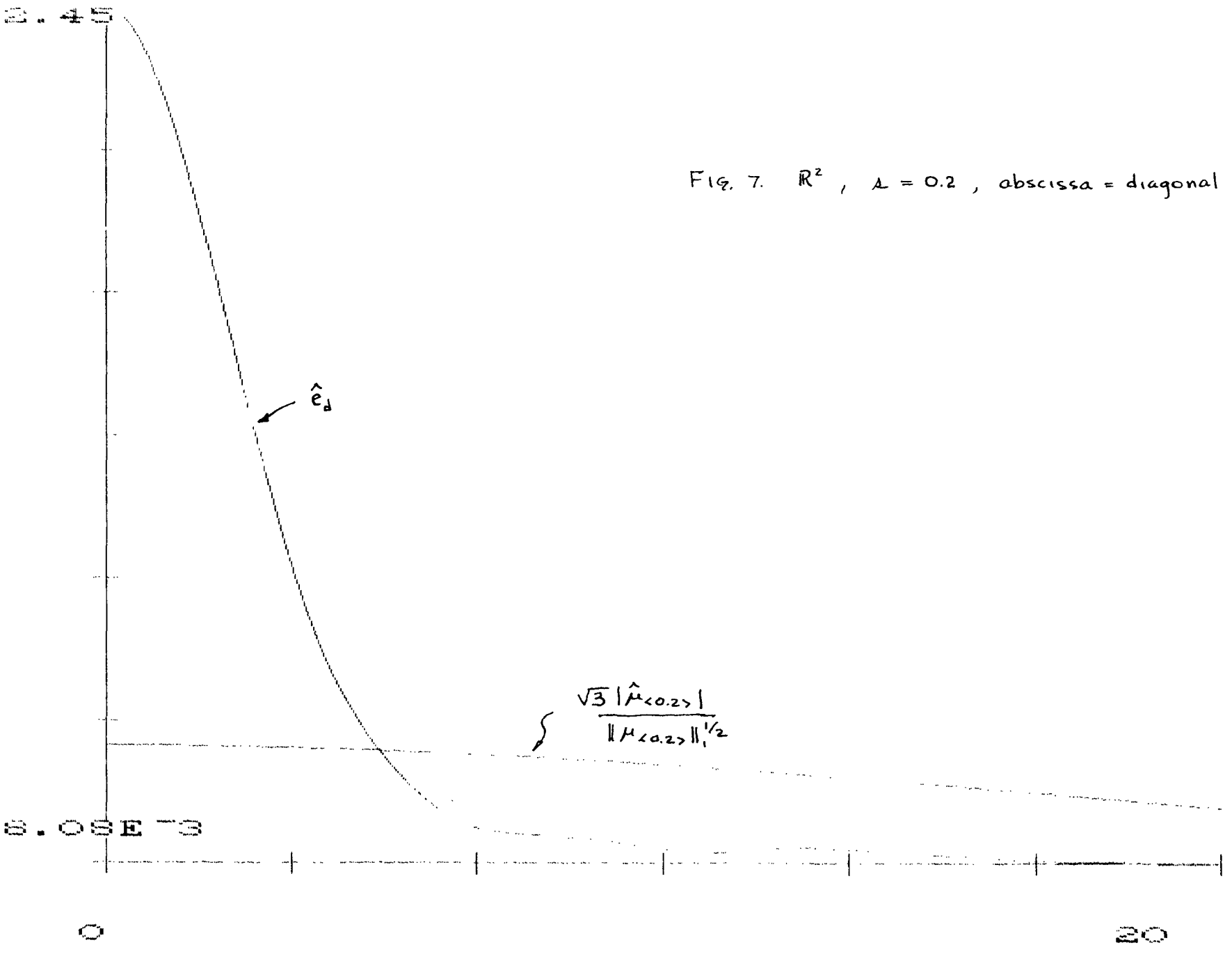

Fig. 7. $\mathbb{R}^2$, $\Delta = 0.2$, abscissa = diagonal

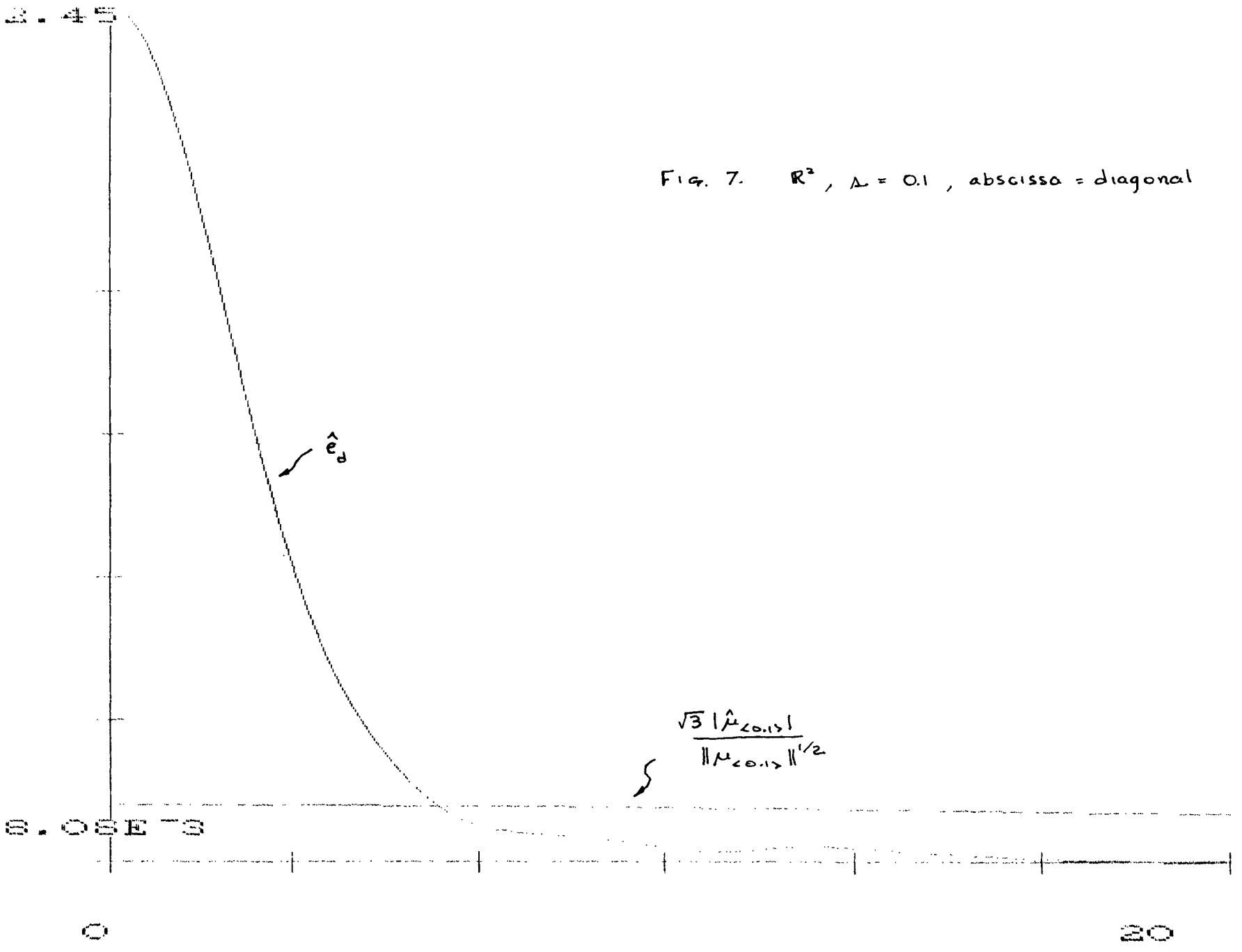

Fig. 7. $\mathbb{R}^2$, $\Delta = 0.1$, abscissa = diagonal

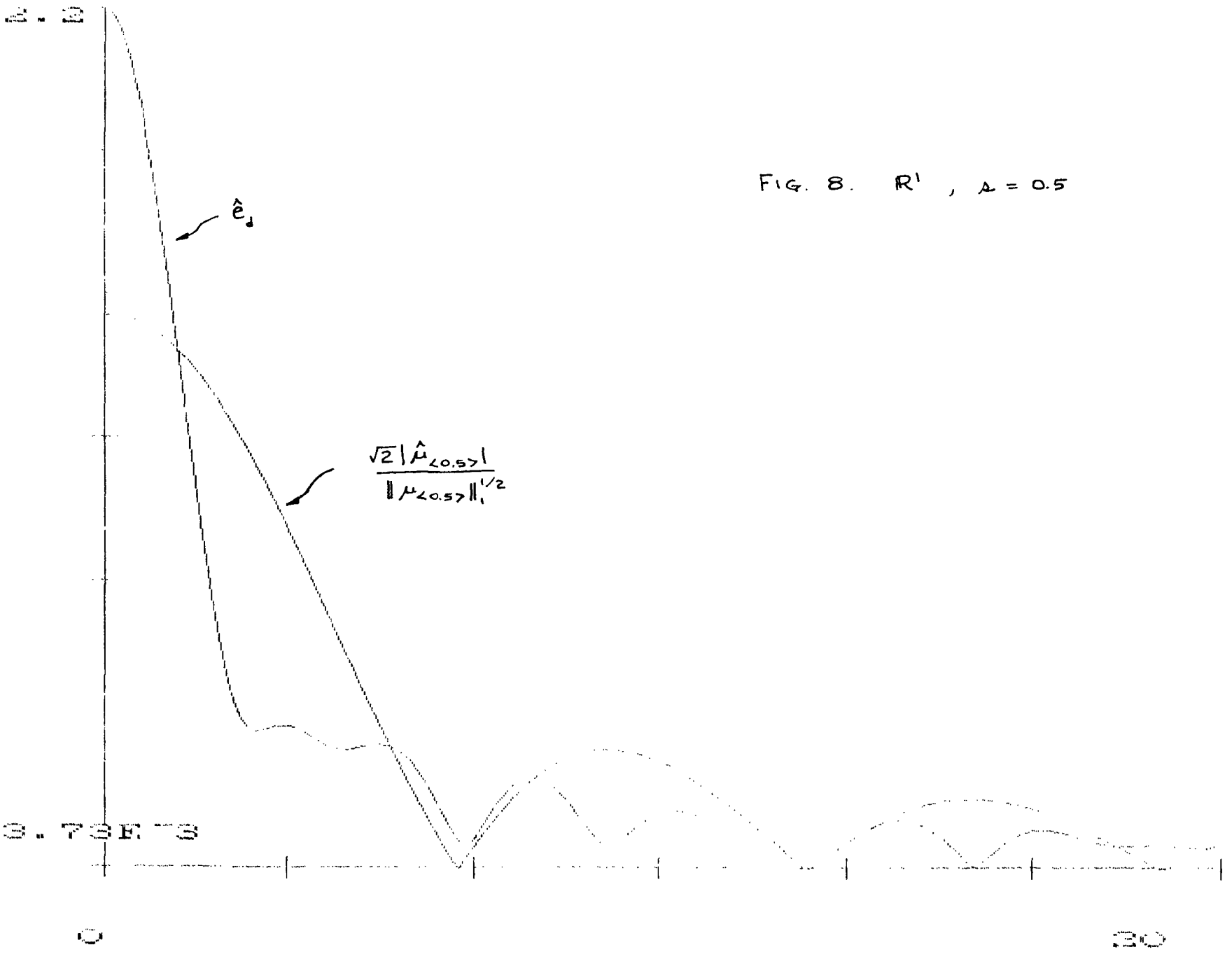

FIG. 8. $\mathbb{R}^1$, $\Delta = 0.5$

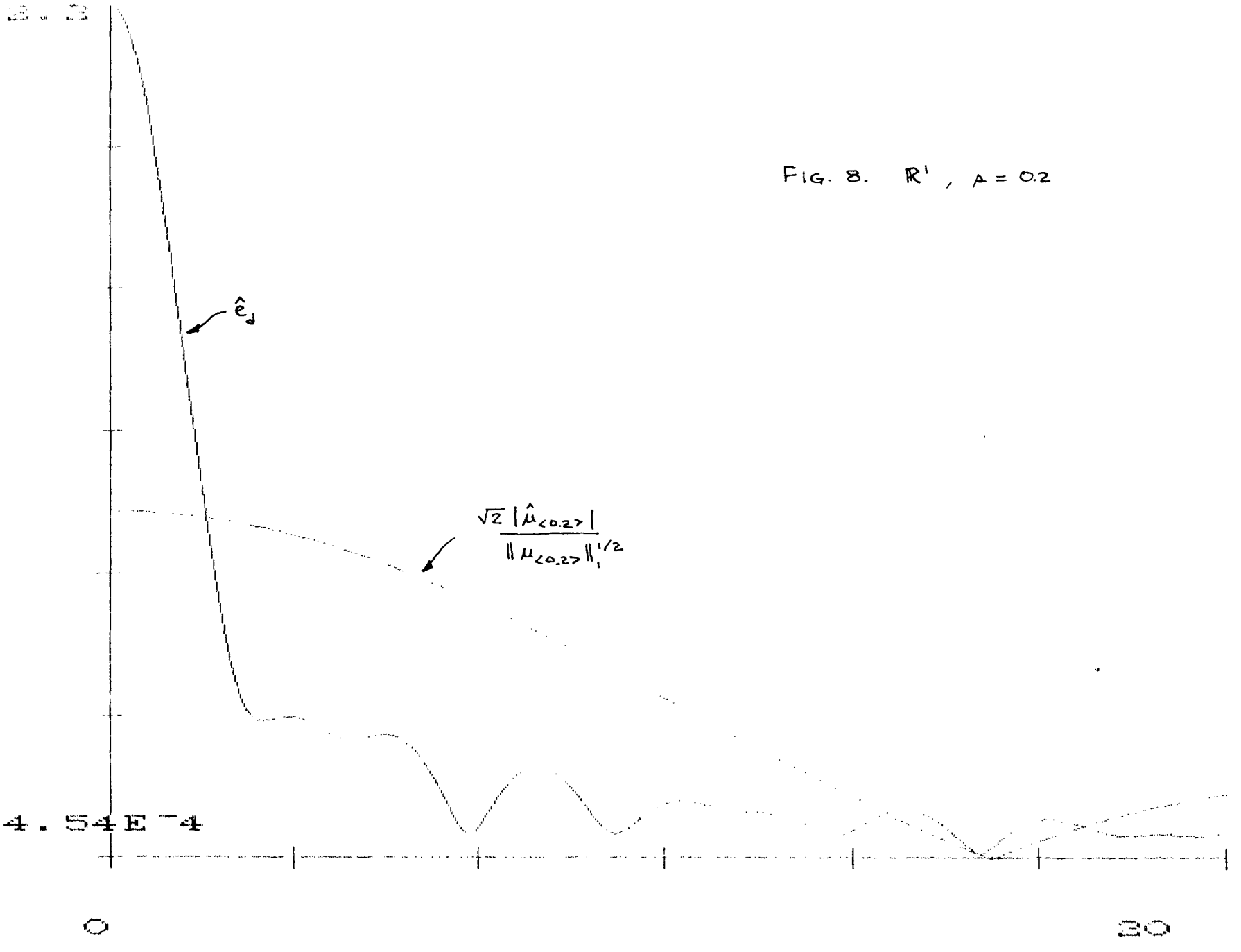

FIG. 8. $\mathbb{R}^1$, $A = 0.2$

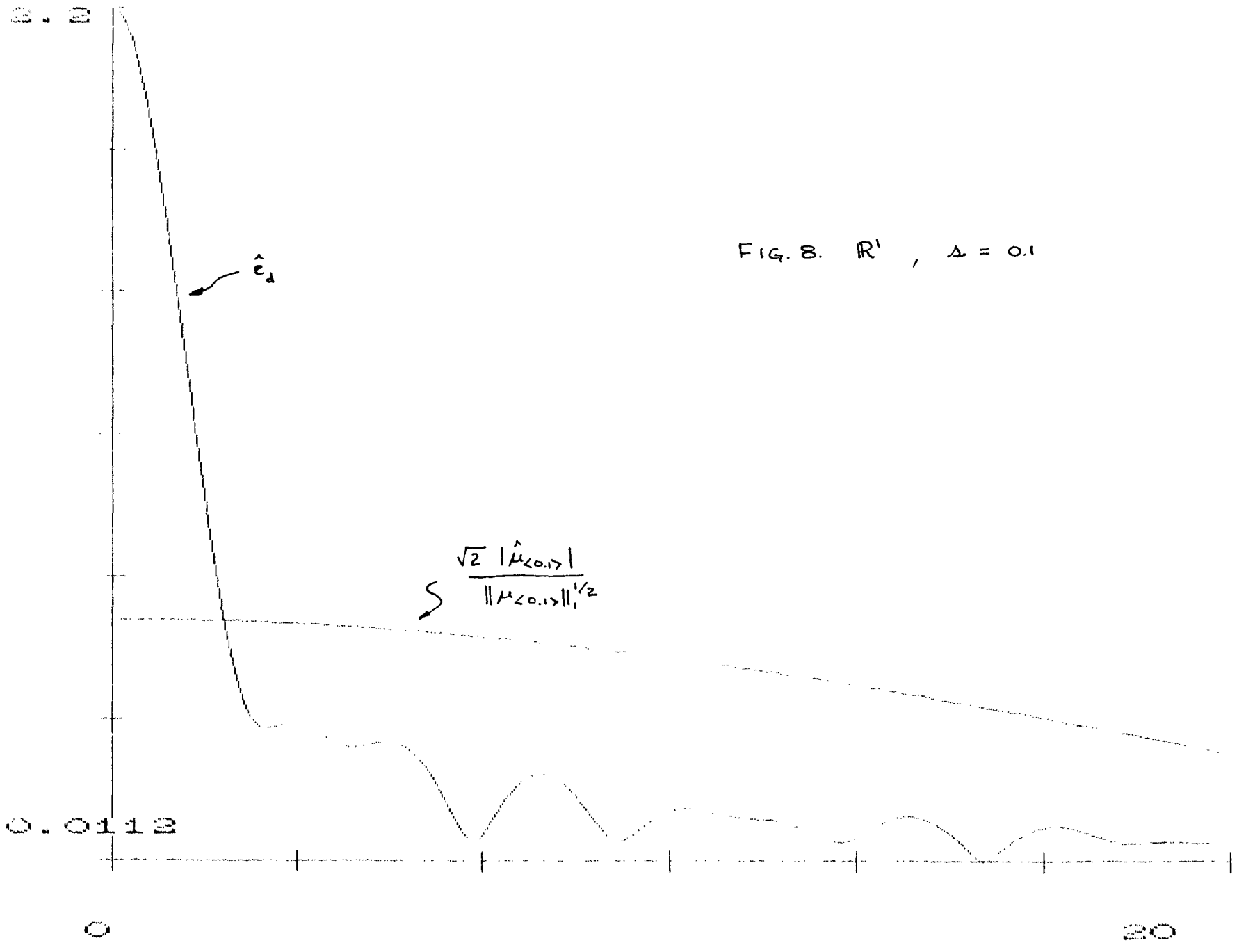

FIG. 8. $\mathbb{R}^1$, $\Delta = 0.1$